Impact of Relative Humidity and Length-scale on the Performance of a Large PEM Fuel Cell

K. K. Lai*, Muhammad Arif*, John Andrews* and Sherman Cheung*‡

*School of Engineering, RMIT University, Australia

(murphylai@vtc.edu.hk, muhammad.arif@rmit.edu.au, john.andrews@rmit.edu.au, chipok.cheung@rmit.edu.au)

‡ Corresponding Author; Sherman Cheung, School of Engineering, RMIT University, Bundoora, VIC 3083, Australia,

Tel: +61 3 9925 6116, Fax: +61 3 9925 6108, chipok.cheung@rmit.edu.au

Received: 11.10.201 Accepted:29.10.2021

Abstract- Polymer Exchange Membrane Fuel Cell (PEMFC) is emerging as a promising candidate for the future power source. Research works have been focused on small PEMFCs while its scalability and performance of large cells remain elusive. This paper presents a numerical investigation on the practicality of expanding a small PEMFC to a large one and a parametric study on the impact of relative humidity (RH) on the operational performance of the large cell. Numerical predictions are firstly validated against our in-house experimental measurements where the predicted polarization (V-I) curve is in good agreement with the measurements. Numerical results confirm that water accumulation/flooding exhibits different characteristics at different regions, namely the activation, ohmic-loss, and concentration loss regions, and poses significant impacts on the current density production. Numerical results also show the small cell is more susceptible to water flooding in comparison to the large cell under similar operational conditions. Suffering from excessive liquid water, the performance of the small cell is not as good as the large one in the concentration loss region, where a significant increase of current density production is observed. Parametric study on the effect of the humidified reactants on cell performance has been also performed. The increase of RH generally shows an increasing effect on the performance of the cell, while the limitation is found at high RHs (60% and 80%) and low voltage (0.3V) due to the hydration of the membrane and the blockage of reactant delivery.

Keywords PEMFC, water flooding, hydration.

Nomenclature

A	Specific active surface area (m^{-1})
C_p	Specific heat capacity (kJ kg^{-1} K^{-1})
F	Faraday's constant (9.65 x 10^7 C $kmol^{-1}$)
H	Hydrogen
$[H]$	Local hydrogen concentration (kmol m^{-3})
$[H]_{ref}$	Reference value of hydrogen concentration (kmol m^{-3})
i	Transfer current density (A m^{-2})
j	Reference exchange current density per active surface area (A m^{-2})
K	Thermal conductivity (W m^{-1} K^{-1})
M	Mass flowrate (kg s^{-1})
O	Oxygen
$[O]$	Local oxygen concentration (kmol m^{-3})
$[O]_{ref}$	Reference value of Oxygen concentration (kmol m^{-3})
R	Universal gas constant (J K^{-1} mol^{-1})
T	Temperature (K)

Greek letters

γ	Concentration dependence
ρ	Density (kg m^{-3})
σ	Electrical conductivity (ohm^{-1} m^{-1})
η	Surface overpotential (V)
α	Transfer coefficient

Subscripts and superscripts

an	Anode
cat	Cathode

Abbreviations

CL	Catalyst layer
GDL	Gas diffusion layer
PEMFC	Proton exchange membrane fuel cell
RH	Relative humidity
MEA	Membrane electrode assembly

1. Introduction

PEMFC operates at low temperatures and has been regarded as a strong and emerging source for the power generation in future [1]. The technology of PEMFCs has interested people because of its simple construction, versatility, quick response, and broad applications ranging from powering a cell phone to an electrical vehicle [2] or

locomotive [3] or in hybrid mode with photovoltaic system [4, 5] or in modules [6]. Beside its promising use in transportation, it is also a suitable alternative for being used in stationary applications. The fuel cell can also be connected to power converter to increase energy efficiency of the system [7] or energy management system to correct the energy demand [8], or by implementing a PID controller to control the output voltage [9]. Thus, PEMFC is versatile in applications. Nonetheless, water management is known to be crucial to fuel cell performance. Production and transportation of water within the PEMFC are related to numerous factors, including power density, gas channel configurations, the porosity of GDL and CL, and the hydration and dehydration of the membrane. Hossain et al. [10] investigated the water dynamics inside a cathode channel of a PEMFC. They concluded that the arrangement of water pores in the GDL surface is the dominant factor affecting water transport from the GDL to the flow channels. Kim et al. [11] conducted a numerical investigation on straight-parallel PEMFCs and concluded that straight-parallel channels have relatively low pressure drop which is beneficial to automotive operation. Moreover, straight-parallel channels also enhance the flow uniformity within the cell, reducing stresses on the MEA and improving the cell durability. Such overall low pressure drop between the inlet and the outlet was also discussed by Dawes et al. [12] in their study of liquid water flooding. However, the application of the metal foam design in the flow field also enhanced the performance of the fuel cell [13]. Various designs of the flow channels like parallel straight [11, 14, 15], serpentine [16, 17, 18], and interdigitated flow channels [19, 20, 21] were also studied by various researchers.

Aiming to resolve liquid water distribution and flooding under non-isothermal conditions, Wang and Wang [22] presented a fully coupling numerical two-phase flow model to resolve the species transport and the associated electrochemical processes. Shimpalee et al. [23] adopted similar numerical approach to analyze the flooding issue in GDL and its impact on the fuel cell performance. They ascertained that water flooding could decrease the oxygen concentration and increase oxygen concentration gradient and surface overpotentials, sequentially lower the fuel cell performance.

The flow of reactants from the cathode channels to the CL would be limited by the amount of liquid water in the cathode GDL as investigated by Dawes et al. [12]. Excessive water causes flooding in the cell when the liquid water generation rate exceeds the capillary transport of liquid water through the GDL. Thus, the performance of the PEMFC is seriously affected. It is also known that water management is crucial in gas diffusion processes [24]. With all the above considerations, water management is one of the dominant factors that determine the power density of the PEMFC. It is noteworthy that the balance between water production from the oxygen reduction reaction (ORR) and water removal from the gas channels is very important in maintaining the optimum membrane hydration in prolonged operations.

The performance of PEMFC under distinctive operating conditions together with different bipolar plate design was analysed by Iranzo et al. [25]. Their results concluded that the coupled relationship between water and thermal management could not be ignored. The degree of corrosion of the CL also showed significant effects on the performance of V-I curves [26]. Parametric analysis on operations at different RHs are conducted by various researchers. Wang et al. [27] stated that for constant RH at the anode and lower operating voltages, a lower RH at the cathode reduces water flooding. For higher operating voltages, a higher RH at the cathode improves membrane hydration. Both cases can improve the cell performance. Zhang et al. [28] discussed that the lowering from high RH to low RH, the production of current density could be suppressed significantly. Xing et al. [29] studied the combined effects among the factors of stoichiometric flow ratio, RH, and channel length on the PEMFCs. Among different combinations of their studies, channel length poses an increasing effect on the current densities.

1.1. Existing research gap

In summary, previous research works have investigated the significance of water management in the PEMFC performance. Nevertheless, most of the studies focused on small-scale PEMFCs ranging from 5 to 50 cm^2 active area. While these studies have provided some insights into the operation within the small cell, the multiphysics phenomenon could exhibit distinctive behaviour in a larger cell with expanding the reactive surface area. With a larger reactive area, the rate of water production within the cell is also bolstered. Water removal becomes critical to ensure the effective delivery of reactants within the cell. In managing the water content over the membrane, the ideal water distribution should be uniform all over the entire membrane. Its uniformity avoids the drying-out or flooding zones which adversely affect the cell behaviour [16]. Traditionally, a parallel straight flow channel design has a better water removal capability when compared to the corresponding serpentine flow field design. The relative superior performance was attributed by a better consumption of hydrogen and oxygen ions. It also had a better water removal rate in the cathode flow channels. Furthermore, the protonic conductivity through the membrane could be enhanced with uniform water distribution and optimal water concentration in the electrolyte.

1.2. New insight of the present study

There are limited experimental and computational studies on the behaviour, characteristics, and performance of large PEMFCs without the use of stacking from small PEMFCs. Numerous investigations of small PEMFCs (~ 5 cm^2) on different geometric configurations have been conducted with focuses on their current density production, thermal management, water management, and so on. But there is a lack of study to use the findings obtained from the small PEMFC and compare them with the large PEMFC by using the same set of computational parameters and material properties. Some of the studies on the large PEMFCs make use of the method of stacking

[30] in which the flow and diffusion characteristics, as well as the performance of the cell, remain the same as in a single small cell but with multiple effects. These extended performances of the stacked large PEMFCs from the small ones cannot truly represent the performance and operational characteristics inside a large PEMFC without stacking. It is worth knowing the performance of a non-stacking large PEMFC that shares a similar configuration with the small PEMFC. A detailed study on the matching of essential parameters in the small PEMFC has been conducted by RMIT research teams [31] and those essential parameters and matching procedures are used in the present study.

One of the purposes of the present study is to find out the effect on current density by expanding a small cell into a large cell. Through the expansion, multiple headers and extended channel length are adopted in the construction of the cathode channels. Afterwards, the performance of the large PEMFC in comparison to the small one will be discussed. As discussed above, water management in the cell takes a major role in its performance as it affects the hydration of the membrane, transport properties in the cathode electrode. The membrane hydration affects the protonic conductivity thus the migration of H^+ ions from hydrogen side to air side while the transport properties in the cathode electrode influence the removal of liquid water and the delivery of reactant to the reaction site. As of the importance of water management in the cell, cathode reactants at different RHs (20%, 40%, 60%, and 80%) are studied and their influences on the membrane hydration and reactant delivery will also be discussed. For the findings from other researchers [27, 32], the study of RH at 100% shows no positive or even negative effects on the current density production on the performance of the cell. Therefore, it would not be taken into consideration in the present study.

2. Experimental Setup

2.1. Experimental setup

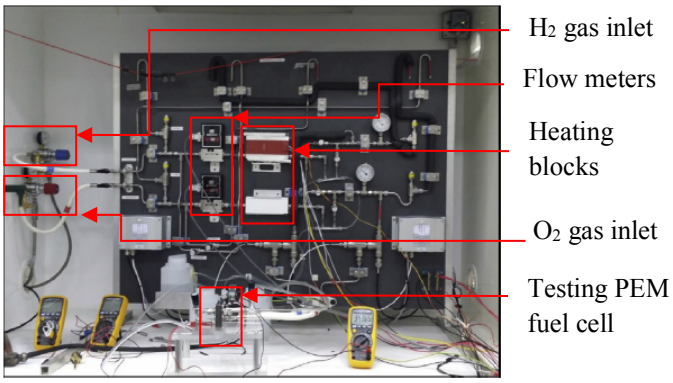

Fig. 1. Experimental setup for the fuel cell measurements.

Figure 1 shows the experimental setup used for the investigation of the PEMFC. The reactants are supplied separately with control by flow meters. The setup is also built up with heating blocks, humidifiers, humidity, and temperature measuring devices for both hydrogen and oxygen.

To ensure the gas pressures will not exceed 1 bar at the reactant entrances of the PEMFC, two separate pressure relief valves are installed in each of the gas lines in the experimental setup. A relatively high pressure (0.9 bar gauge, primarily for air/oxygen) to ensure sufficient reactants are available at the cathode. The PEMFC is maintained at a reasonably high temperature (~ 53°C) to ensure liquid water retention is reduced to avoid water flooding problems, together with assistance in increasing the kinetics of the reaction. No pre-heating of input gases is set before they enter the cell, and the gas flow rates are ranging between 50 to 80 mL min^{-1}. The RH of the gases are close to their ambient condition indoors, which is approximately 13% respectively. The active surface area of the membrane is 225 cm^2 with dimensions of 15 cm × 15 cm. Experimental study on the fuel cell performance under distinctive operating conditions was analyzed by [22]. They also conducted study on different bipolar plate designs. However, humidified reactants or the use of pure oxygen also improved the cell behaviour and resulting in enhanced V-I curves. [33] presented an experimental investigation of PEMFC aging under current cycling using segmented fuel cells and suggested that the surface area of the CL decreased due to water flooding. Another experimental study of the internal resistance of the microbial fuel cell was conducted by [34]. Their study had covered the internal resistances of the activation, ohmic, and concentration loss regions. They concluded that the resistances behave differently under different current densities. [35] conducted experimental study on the V-I curves from single-cell URFCs with different cathode catalysts and compared them with the theoretically modeled curves.

3. Numerical Modelling

ANSYS FLUENT Fuel Cell Module was adopted in the numerical study for resolving the electrochemical reactions. The Butler-Volmer equation used to describe the volumetric transfer current is written as [36]:

$$i_{an} = A_{an} j_{an}(T) \left[\frac{[H]}{[H]_{ref}}\right]^{\gamma_{an}} \left[exp\left(\frac{\alpha_{an}^{an} F\eta_{an}}{RT}\right) - exp\left(\frac{-\alpha_{cat}^{an} F\eta_{an}}{RT}\right)\right] \quad (1)$$

$$i_{cat} = A_{cat} j_{cat}(T) \left[\frac{[O]}{[O]_{ref}}\right]^{\gamma_{cat}} \left[-exp\left(\frac{\alpha_{an}^{cat} F\eta_{cat}}{RT}\right) + exp\left(\frac{-\alpha_{cat}^{cat} F\eta_{cat}}{RT}\right)\right] \quad (2)$$

Identical to the experimental fuel cell, a 3-D computational PEMFC model was constructed. The height of channels is 1 mm while the width of headers and the straight parallel channels are 2 mm and 1 mm respectively. The dimensions of flow channels are 1 mm by 1 mm, the thickness of cathode GDL, cathode CL, membrane, anode CL, and anode GDL are 0.1 mm, 0.01 mm, 0.03 mm, 0.01 mm, and 0.454 mm respectively. Inlet and outlet boundaries of the hydrogen/air are considered after the pressure relief valves. Figure 2 shows the computational model for the gas channels at the anode and cathode electrodes. A hybrid tetra-hexahedral mesh was generated to discretize the computational domain. In general,

structured hexahedral mesh were generated for the gas channel and the vicinity area.

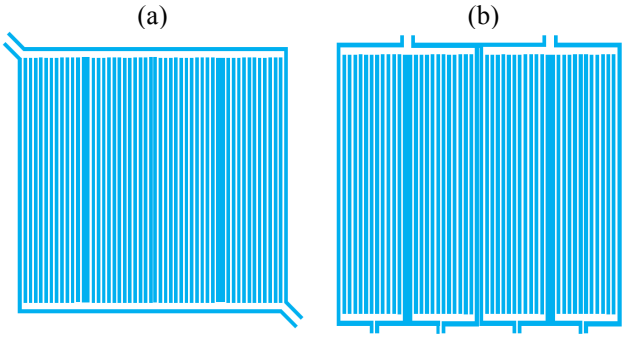

Fig. 2. Gas flow channel configurations for (a) anode; and (b) cathode.

A grid sensitivity test has been carried out to ensure numerical predictions are mesh independent. Three different sets of mesh resolution were tested where the amount of mesh across the MEA (i.e., from the GDL to the CL and the membrane) are 13-2-10, 15-4-12, and 17-6-14, respectively. The varied structures were simulated against the voltage at 0.51V to check the difference in the values of current densities. Upon the increase in grid layers in the MEA, the amount of time to get the simulations converged increases significantly more than 3 times for simulations to be conducted in a PC. The results showed that the difference in current densities among the three sets of layers was negligible. Therefore, for the sake to minimize the amount of computational time required for converged solutions with minimum deviation, the 15-4-12 numbers of grid layers were adopted in subsequent simulations.

Table 1. Properties of the PEM fuel cell layers.

	$\rho \times 10^3$	$C_p \times 10^2$	K	σ
Electrolyte	1.97	20.0	2.00	1.0×10^{-16}
Anode CL	2.72	8.71	10.0	5.0×10^3
Cathode CL	2.72	8.71	10.0	5.0×10^3
GDL_{an}	37.7	8.71	10.0	2.7×10^5
GDL_{cat}	1.35	5.20	21.9	2.4×10^6
Collectors	8.00	5.00	16.3	1.4×10^6

Table 2. Physical parameters of the numerical model.

Parameters	Conditions
Operating pressure, [Pa]	1.01×10^5
M_{H2} at anode flow channels, [kg s^{-1}]	5.00×10^{-6}
M_{O2} at cathode flow channels, [kg s^{-1}]	2.00×10^{-5}
Porosities of GDL_{an} and GDL_{cat}	0.63
Porosities of CLs	0.28
Mass fractions of H_2	0.96
Mass fractions of O_2	0.21
T_{an} and T_{cat}, [K]	326
V_{cell}, [V]	1.10

The set of equations were solved by ANSYS FLUENT Fuel Cell Module. SIMPLE algorithm and 1st order upward were adopted to solve the pressure-velocity coupling and the convection terms. The convergence criteria of the governing equations are set to be 1e-6. To compare with the experimental measurements, steady-state simulations were carried out and the boundary conditions for both gas channels were set according to the experimental conditions. The characteristics of the cell layers and the physical parameters adopted in the simulations were identical to the experimental conditions which are tabulated in Tables 1 and 2, respectively.

4. Results and discussions

4.1. Numerical model validation

The numerical model was constructed based on the experimental setup and design of the fuel cell with multiple long channels in both anode and cathode electrodes. The comparison of the V-I curves between the experimental measurements and numerical predictions of the large PEMFC is shown in Fig. 3.

According to Huang et al. [37], the V-I curve can be classified into three main regions: activation loss, ohmic loss, and concentration loss regions. As depicted, the numerical predictions are in excellent agreement with the experimental measurements. One could observe that the initial rapid drop in the activation loss region and the sequential steady drop in the ohmic loss region are adequately captured by the numerical model. In the concentration loss region, the current density is slightly under-predicted by 2.54% compared to experimental data. The first drop of the V-I curve indicates the required energy to activate the electrochemical reactions within the cell. The activation energy is to overcome the ohmic resistance to facilitate ions transfer within the cell. Once the cell is activated, the V-I curve exhibits a steady drop in the ohmic loss region, indicating a gradual increment of cell power output.

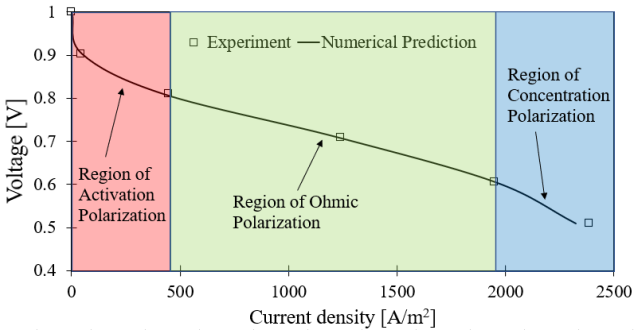

Fig. 3. Comparison between the experimental and numerical predicted V-I curves.

Meanwhile, as water is the by-product of the electrochemical reaction, it started to accumulate in the cell layers in both liquid and water vapor forms. In the concentration loss region (i.e., low voltages operation), the production and retention of water in the reaction sites prevailed its removal rate via gas channels. As a result, as it was mainly driven by the diffusion process, excessive water started to accumulate in the CL and GDL in the cathode side of the cell. The accumulated water eventually caused flooding in the electrode and hindered the

electrochemical reaction rate by blocking oxygen from reaching the reaction site. Sequentially, the blockage of water decreased the current density and the performance of the fuel cell. As discussed above, a slight under-estimation of the current density can be observed at the low supply voltages in the concentration loss region. The prediction errors could be referenced to the over-estimation of the saturated liquid water retained in the cathode electrode, under-estimating the diffusion rate of oxygen through the GDL to the CL. The above findings agreed with our experimental observations.

During our experiment, a certain amount of liquid water was observed dripping out from the boundaries of contacting surfaces of the cell in the experimental setup, and on some occasions, purging of the channels was implemented to remove water from the channels and to increase the airflow rate. The way of water squeezing out from the cell during the experiment was explicitly captured in the current computational model. In the present model, water removal from the cell is only considered as a water vapor mass transport process diffusing through the CL, GDL and eventually to the gas channels. The lack of water droplet consideration could constitute an error in predicting the water content in the cathode electrode compared to the experimental data. The prediction errors could become considerable at high current density operations where relatively higher water content is produced in the cell. In general, only minor prediction errors were found in this study. It can be concluded that the numerical model adopted in this study can accurately capture the electrochemical reactions within the cell and its associated performance under various voltage potentials.

4.2. Performance comparison between the small and large PEMFCs

Aiming to investigate the scalability of the fuel cell, this paper also compares the performance of the cell by expanding the active area from our small-scale to the present large-scale model. The large PEMFC is generally the expansion from the small PEMFC in the RMIT fuel cell laboratory, they are both parallel straight channels with multiple headers. For the small PEMFC, the parallel straight channels originate from common headers at both ends. While multiple parallel straight channels of the large PEMFC originate from separate headers and ends with separate headers. The dimensions of the channels of both cells are 1 mm (width) by 1 mm (height) while the straight sections of the large cell are extended about 7 times compared with the small cell. The channel cross-sectional area (i.e., width and height) are maintained while the length is extended. The multiple extension of the channel length is expected to cause a higher pressure drop, adding an efficiency penalty in hydrogen/air delivery. Besides the changes in geometry to cater for the flow characteristics between the small and large PEMFCs, all other physical parameters, material properties and numerical settings are kept the same as listed in previous tables. Moreover, the operation conditions of the gases between the small and large PEMFCs are also identical, such as RH, temperature, and properties, etc.

The comparison of the V-I curves between the small and large PEMFCs is shown in Fig. 4. It is observed that a slightly higher current density production was obtained with the small cell at high supply voltages. Meanwhile, the performance is reversed at lower supply voltages with a turning point at the voltage of 0.8V. As discussed before, the rate of electrochemical reaction is relatively slow at high voltages due to the activation energy. A slower rate of water production results in both large and small cells and the RH of cathode reactants of these simulations is 34%. So, the amount of water in the cathode electrode at activation polarization is small. Owing to its expanded size, the capability of water uptake in the membrane of the large cell is relatively larger than the small cell. It is well-known that the hydration of the membrane takes an important role in proton conductivity [38]. The amount of hydrogen ions (H^+) in the cathode electrode has a crucial effect on the ORR so as the production of water in the electrode. Therefore, the level of hydration in the membrane in the small cell could be higher than that in the large cell, leading to a higher current density production during the activation polarization. Once the rate of electrochemical reaction is enhanced at low voltages after overcoming the activation loss and come into the ohmic and concentration loss regions, more water is produced and dissolved into the membrane and thus the protonic conductivity is also enhanced and the formation of water from the ions is increased. At this moment, the amount of water in the large cell at the cathode electrode is higher than that in the small cell. Therefore, current density production is improved with a greater portion for the large cell than the small cell. The impact on the water saturation and mass fraction of oxygen between the small and large PEMFCs will be discussed in later sections.

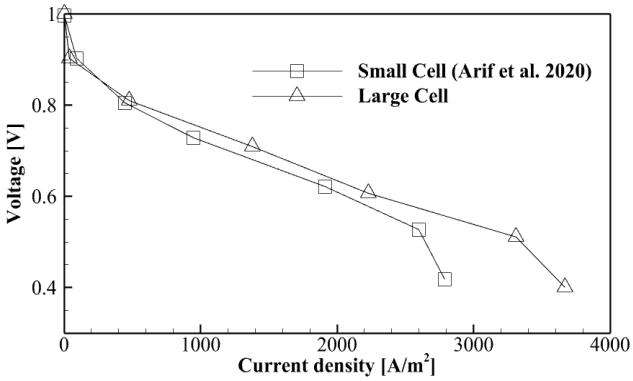

Fig. 4. Comparison of V-I curves between the small [31] and large PEMFCs.

4.3. Water saturation distribution between the small and large PEMFCs

As water is formed in the electrochemical reaction, it diffuses out from the CL through the GDL to the channels. The contour of liquid saturation at the interface between the GDL and the channels shows differently in their contents (Fig. 5). In the small PEMFC, liquid water is found in the interface while negligible liquid water is found in the interface of the large PEMFC. However, the volume-averaged liquid saturation in the GDL of the large

and small cells are 7.1×10^{-18} and 0.074 respectively. With identical material and operation conditions, the numerical predictions suggest that the extended geometrical configuration of the large cell can enhance the removal of water through the cathode channels in comparison to the small cell.

It will become more apparent in the coming sections that liquid water would not accumulate in the large cell until the inlet reactants are humidified to 40% RH or above. Thus, in comparison to the configuration of the small fuel cell, the multiple long channels design with separate headers are more susceptible to removing water away from the cell. According to the geometry, the large cell is constructed with four sections with long channels and each section has its outlet while the small cell has only one outlet. Also, the velocity profile inside the cathode channels is quite steady and uniform in the large cell. This indicates the extended straight portions of the long straight channels help to stabilize the flow inside the channels. As a result, more liquid water was removed from the cell, retaining less liquid water within the cell. Reactant's transportation in the large cell is more effective and the cell performance is enhanced.

Figure 4 shows a large difference in current density between the large and the small PEMFCs at the voltage of around 0.5V. The difference may be affected by the degree of hydration in the membrane as hydration helps to improve the proton conductivity. Figure 6 shows the water content in the membrane at 0.5V. It can be observed that the membrane water content in the large PEMFC exhibits a better distribution over the membrane when it is compared with the distribution of the small PEMFC. The water content of the large cell distributes evenly from the inlet to the outlet. However, the water content in the small cell distributes unevenly over the membrane with more water concentrated on the lower and middle part of the membrane. The area-averaged values of water contents in the small and large cells are 8.25 and 8.61 respectively which shows that the membrane hydration is better in the large cell than the small cell. The enhanced hydration in the membrane promotes a better protonic conductivity through the membrane.

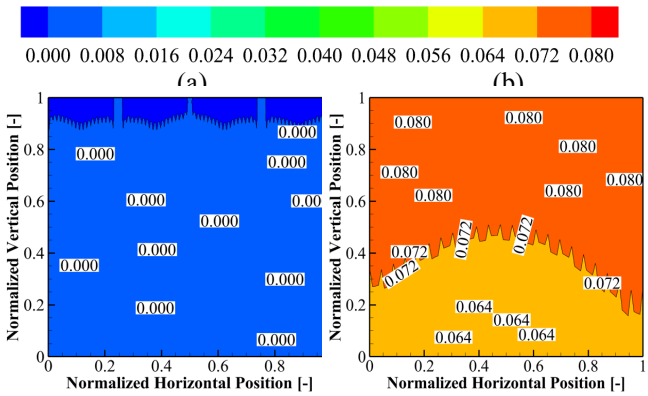

Fig. 5. Water saturation at the interface between cathode GDL and channel at 0.5V of a) large PEMFC; b) small PEMFC.

4.4. Exploration of RH on the overall cell performance

As discussed in the previous section, water saturation could hydrate the membrane and enhance the protonic conductivity and the overall cell performance. On the other hand, excessive saturated water could also pose a hindrance to reactants' transport through the GDL, causing a barrier to the electrochemical reaction.

Several researchers have attempted to adopt different membrane materials or impair hydrophobicity in the GDL to remove additional water content [30, 38, 39]. By altering the content of the Polytetrafluoroethylene (PTFE), Chun et al. [40] concluded that the PTFE could act as a hydrophobic agent in the microporous layer and improve the performance of a single fuel cell by enhancing a more effective water removal. Shimpalee et al. [38] investigated the effect of membrane material properties on mass transports and its associated performance of the PEMFC. They concluded that hydrocarbon membranes could have a better performance at high humidity conditions, while conventional Nafion membranes could perform better at low humidity conditions due to their inherent characteristics of higher water diffusivity and electroosmotic drag coefficient. Their studies ascertain that RH of the supply air could pose a significant impact on the water content and the fuel cell performance. To further examine the influence of RH, a parametric study of different levels of humidification on cathode reactants was carried out based on the parallel long straight channels configuration of a large PEMFC.

Consistent with the validation above, all operation parameters remain unchanged except the RH level as the sole changing parameter. Figure 7 shows the predicted V-I curves for cathode reactants at different RH conditions for the identical experimental large PEMFC. In general, across different RH values, the patterns of the V-I curves are similar for all activation, ohmic, and concentration loss regions. As depicted, one can observe that a higher RH reactant level generally resulted in a higher overall current density and cell performance. Noticeable performance deviations start to take place at 0.8V with increasingly widened deviation in current density down the decreasing voltages until 0.3V. Figure 7 shows that the humidified reactants pose a substantial effect on the current density generation of the cell. Nonetheless, at high humidified reactants (i.e., 80%), the V-I curve behaved very close to 60% humidified reactants especially at low voltages, 0.3V. Such a minor difference indicates that the degree of enhancement in current density production is not as prominent as those below 60% RH. It can be seen in the later section that higher humidified reactants lead to higher membrane water contents which promote proton conductivity and thus boost the electrochemical reaction and current density production.

4.5. Local RH distribution in cathode channels

Figure 8 shows the contour of the RH distribution in the cathode channel corresponding to four different RH reactant conditions at 0.3V. In general, align with the gas flow, the RH distribution appeared to be minimum at the inlet and gradually increased towards the outlet of cathode channels. Although different RHs were supplied at the

inlet, similar contour patterns were observed for the four cases. Compared to the supplied RH at the inlet, the water accumulation increased more at low supply RH than high supply RH before its saturation at 100% throughout the multiple long channels to the outlets. The RH increment indicated the gradual addition of water vapor from the inlet to the outlet via diffusion process through the GDL into the gas channels. In other words, the increment of RH poses positive effects on the oxygen consumption rate and electrochemical reactions. Saco et al. [41] showed that in his scaled-up model of 225 cm^2, better oxygen consumption is obtained in parallel straight channels when compared with serpentine channels. It also showed that the straight parallel channels result in low water concentration in the channel, GDL, and CL.

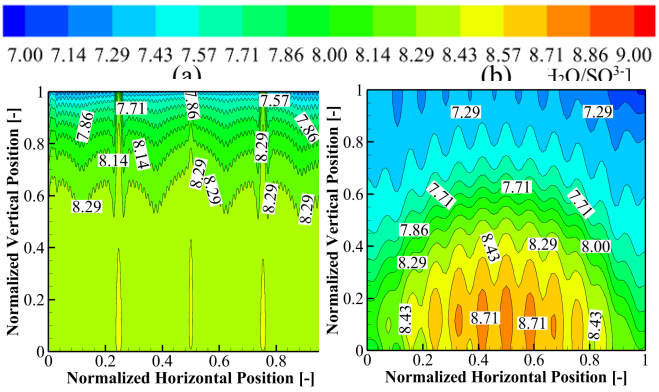

Fig. 6. Water content in the membrane at 0.5V of a) large PEMFC; b) small PEMFC.

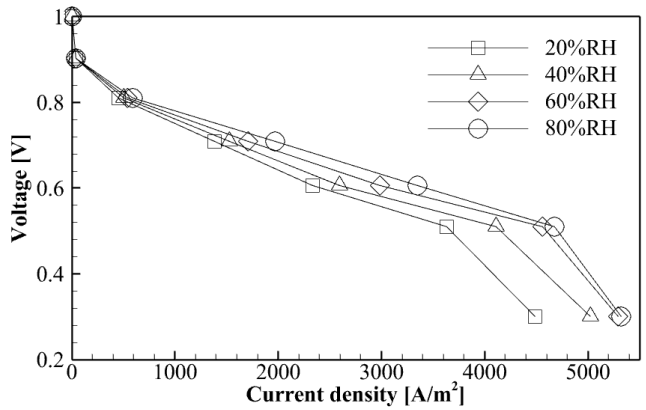

Fig. 7. Polarization curve at various RH at cathode inlet.

4.6. Impact of membrane water contents on current density and cell performance

Figure 9 shows the predicted local current density distributions at the CL for four different RH conditions at 0.3V. As depicted, for lower RH conditions (i.e., 20% to 40%), a gradual increasing current density pattern can be observed starting from the cathode gas channel inlet (i.e., top of the figure) to the vicinity of the channel outlet (i.e., bottom of the figure). On the other hand, the characteristic of the current density distribution exhibits considerably distinctive features for higher RH conditions ranging from 60% to 80%. Table 3 shows the variation of the area-averaged current density between the upper and lower parts of the membrane at different RH conditions. It indicates that the highest spatial variation (i.e., 10.31%) is found at 40% RH. The reason could fall into the difference in water contents in the membrane and cause a larger variation in protonic conductivity which would be discussed later (Fig. 10). Regarding the increased humidification of the cathode reactant, the change in percentage for the lowest RH is also displayed in Table 3. Increasing the RH from 20% to 80% poses an enhancement of 23.96% in current density in the membrane. Indicating an improvement in the overall performance of the PEMFC (see also in Fig. 7). The increased RH from 60 to 80% cannot significantly booster the reaction rate and only the upper part of the membrane can benefit from the effect of increased RH. But the degree of enhancement is very small. This would be related to the water contents in the membrane. More evidence can be found in a closer examination of the saturated water content at the CL.

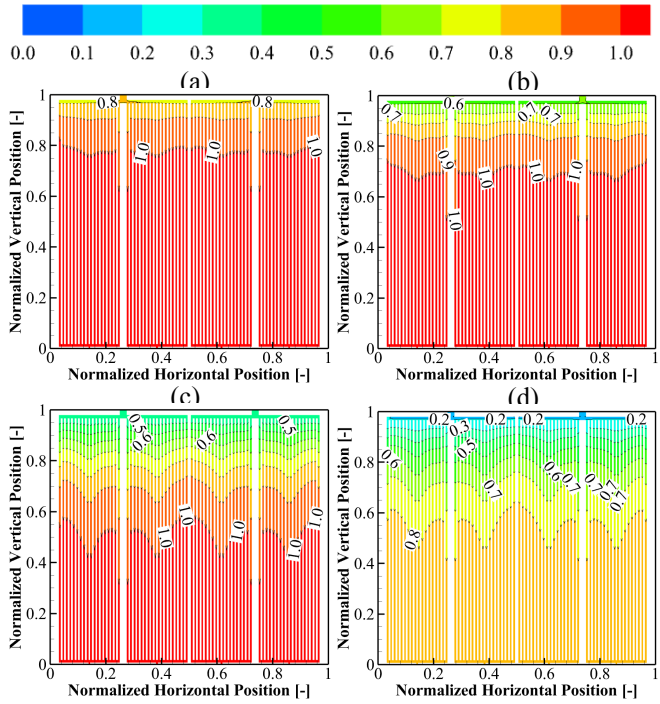

Fig. 8. Contour of RH in cathode gas channels at 0.3V: a) 80%, b) 60%, c) 40%, d) 20%.

Figure 10 shows the predicted local water content distribution in the membrane for different RH conditions at 0.3V. Similar to the RH distribution within channels, there is an increasing trend of water content in the membrane spanning from inlet towards outlet for RH conditions below or equal to 60%. At 60% RH, almost the entire membrane has been occupied by saturated water, indicating a high level of water saturation in the membrane. Further increasing the RH value to 80% shows a different water content distribution over the entire membrane. As a high level of water saturation starts from 60% RH, water content becomes fully saturated in the membrane at 80% RH, leading to insignificant enhancement of current density and electrochemical reaction (see also in Fig. 7). As evident, the water

saturation affects the electrochemical reaction starting from 60% RH and hinders the electrochemical reaction and increment of current density as shown in Fig. 7. At 80% RH, the local variation of water content is practically insignificant compared with other RH conditions. It ascertains that the rate of water removal from the reaction site is slower than the water production caused by electrochemical reactions. Water content in the entire membrane is therefore fully saturated. It is believed that the highly saturated water content poses a great hindrance to the electrochemical reaction/ORR. Thus, the current density distribution has been increased as compared to those at lower RHs (40% and 20%). Thus, the proportion of the increase in current density from 60% to 80% RH is not as great as those from 40% RH to 60% RH or even lower RHs.

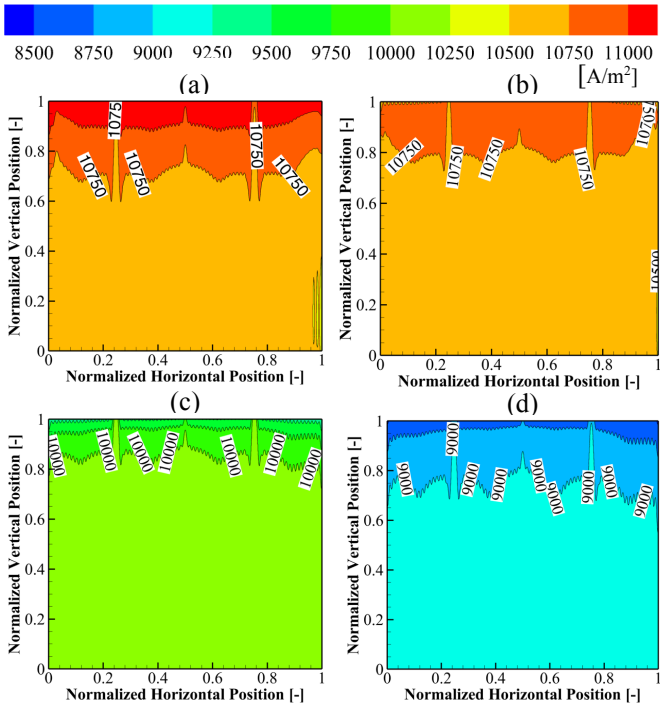

Fig. 9. Variation of current density in membrane at 0.3V: a) 80%, b) 60%, c) 40%, d) 20%.

Table 3. Variation of current density in the membrane at 0.3V.

RH of air	I_{max} [A/m²]	I_{min} [A/m²]	ΔI [%]	$\Delta I_{w.r.t.\ 20\%RH}$ [%]
80%	11329.90	10478.30	8.13	+23.96
60%	10931.40	10489.60	4.21	+21.76
40%	10201.00	9247.84	10.31	+10.55
20%	9140.76	8451.65	8.15	0.00

Figure 11 shows the predicted local water content distribution at 0.5V under all different RH conditions. Comparing to the low voltage (i.e., 0.3V) condition, a progressive accumulation of water content over the entire membrane can be observed from low to high RH conditions. It is worth noting that there is a slight increment in water content from 60% to 80% RH conditions, although such increment is noticeably higher than the one at 0.3V. The predicted results reveal that the humidification of cathode reactants brings an insignificant influence on the water content in the membrane starting from 60% to 80% RH in this large cell.

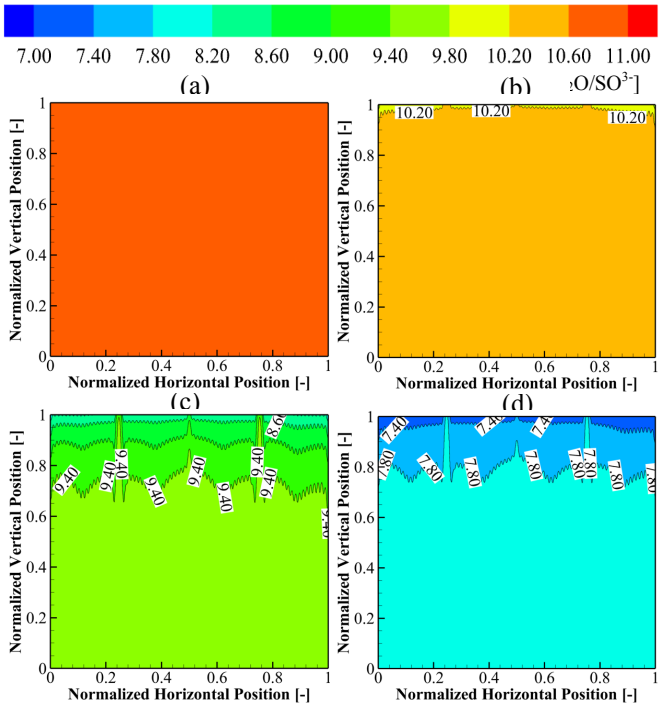

Fig. 10. Variation of water content in membrane at 0.3V: a) 80%, b) 60%, c) 40%, d) 20%.

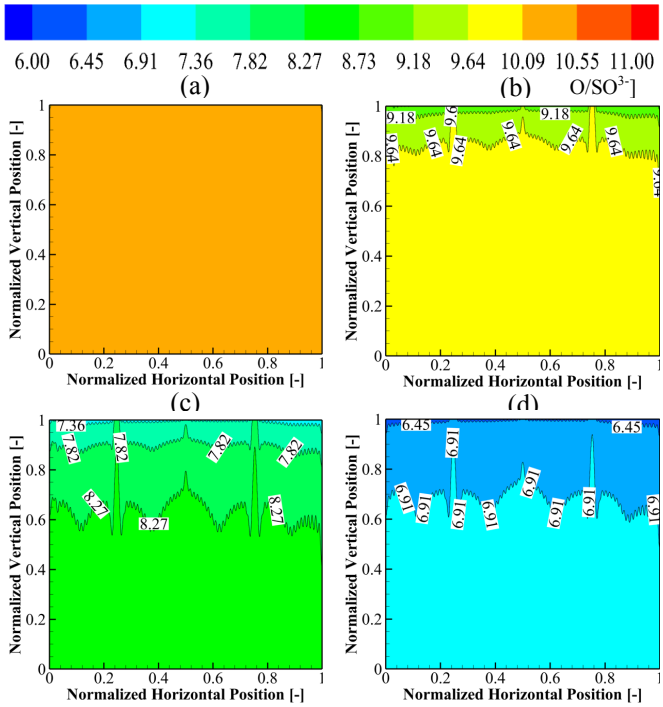

Fig. 11. Variation of water content in membrane at 0.5V: a) 80%, b) 60%, c) 40%, d) 20%.

According to Springer et al. [42], the properties of the membrane are evaluated as functions of the water content. Those inherent properties include the water diffusivity, the osmotic drag coefficient, and the electrical conductivity.

The increase in water content enhances the membrane conductivity, and the proton transport through the membrane, reducing the ohmic loss in the cell. Although hydrating the membrane could be beneficial to the cell performance, an excessive amount of liquid water could also hinder the cell performance in the mass transfer region by blocking the gas diffusion process and the effective reacting surface area, leading to a reduction of reaction rate.

The partial pressure of water vapor is increased with the increased RH of the cathode reactants, and this would bring an increased water activity in the CL by bringing to a higher equilibrium water content. Thus, the amount of water accumulation in the membrane is increased. The presence of water blocks the passage of the reactant diffusion to the reaction site by decreasing the diffusion rate and the effective reacting surface area and therefore would reduce the cell performance [32].

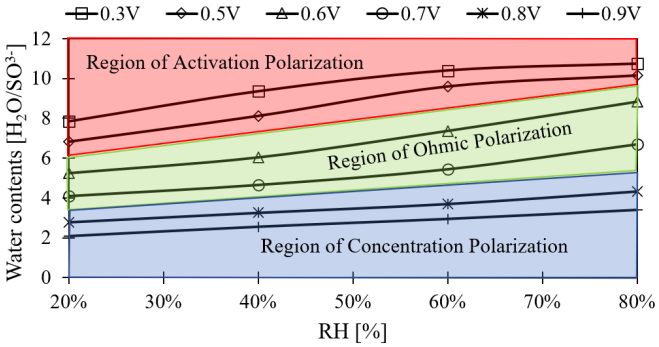

Fig. 12. Water contents in the membrane at different RHs.

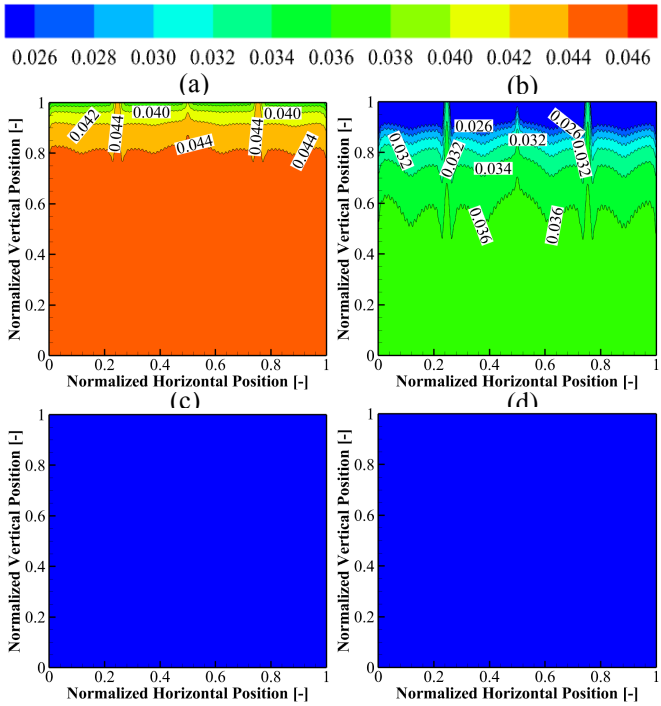

Fig. 13. Variation of liquid saturation in CL/GDL interface at 0.3V: a) 80%, b) 60%, c) 40%, d) 20%.

Figure 12 shows the resultant membrane water contents at different RH conditions. As discussed above, higher membrane water content is observed at higher humidified cathode reactants. Depends on the corresponding loss regions, one could observe the difference in water absorption levels in the membrane. Compared to low RH conditions, the amount of water content at high RH conditions (i.e., 60% to 80%) exhibits an insignificant increment and impact on the cell performance within the activation loss region (i.e., 0.8V and 0.9V). A noticeable jump of water content can be observed for the ohmic loss region (i.e., 0.6V and 0.7V). The additional water content provides hydration of the membrane and sequentially reduces the ohmic loss of the fuel cell; leading to a substantial enhancement of current density comparing to low RH conditions (see also in Fig. 7). In the concentration loss region (i.e., 0.3V and 0.5V), the increment of water content is also substantial compared to the low RH conditions. Nonetheless, as discussed above, the water content in the membrane also becomes saturated after 60% RH. In general, driven by electrochemical reactions, the decrease in supply voltages enhances the resultant current density. More water is thus dissolved into the membrane, indicating a tendency of enhanced protonic conductivity through the membrane and better performance of the cell. The increasing trend of water content is found to consistently occur at all RH conditions (i.e., from 20 to 80%). It is also worth noting that similar findings of water absorption are also reported by [38].

4.7. Water saturation and its effect on reactant transfer

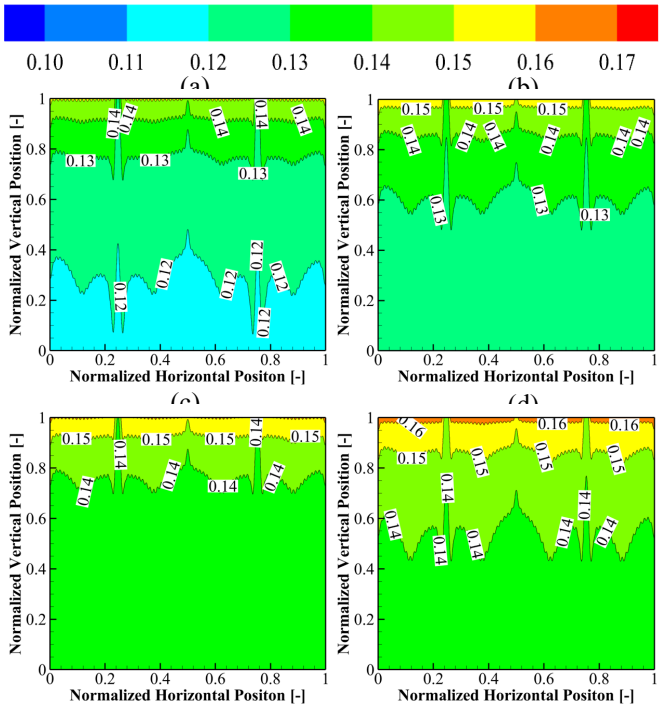

Fig. 14. Variation of mass fraction of oxygen in CL/GDL interface at 0.3V: a) 80%, b) 60%, c) 40%, d) 20%.

Figure 13 shows the predicted liquid saturation at the interface between the cathode CL and GDL at 0.3V under all different RH conditions. For the high RH (i.e., 80% RH) case, as depicted, liquid water formed in the CL accumulated and distributed all over the entire area of the interface between the cathode CL and GDL. Liquid

saturation at the interface decreases from 80% RH to 40% RH in which only the bottom half of the interface is filled up with liquid water. This indicated that the reaction rate at 40% RH and 0.3V voltage forms less water in comparison with other reactants with higher RHs, and the interface is not flooded with liquid water. This could attribute to the lower partial pressure of water vapor at low RH cases, causing less liquid water formation in comparison to those at high RHs. Thus, the liquid saturation is lowered. For the sake of lowered liquid saturation, the amount of liquid water being absorbed by the membrane is also lowered. As discussed above, the decreased membrane water content leads to decreased protonic conductivity in the cell and thus the performance of the cell. Further reducing cathode reactant to 20% RH, the formation of liquid water is insignificant, and the performance of the fuel cell is further reduced.

As of the differentiation of liquid water at the interface between cathode CL and GDL discussed above, a closer examination of the mass fraction of oxygen at that interface is shown in Fig. 14. For the 80% RH case, the corresponding mass fraction of oxygen at the interface is the lowest among all cases. Decreasing the RH value of the cathode reactants shows a progressive increase in the mass fraction of oxygen available at the interface. This indicates that the presence of liquid water at the interface plays a role in the oxygen delivery to the interface and its availability for the electrochemical reaction. On the other hand, though the mass fraction of oxygen is changing, its distribution patterns at different RHs are similar. A higher amount of oxygen can be observed at the vicinity of the cathode inlet, while a lower amount of oxygen is found at the cathode outlet.

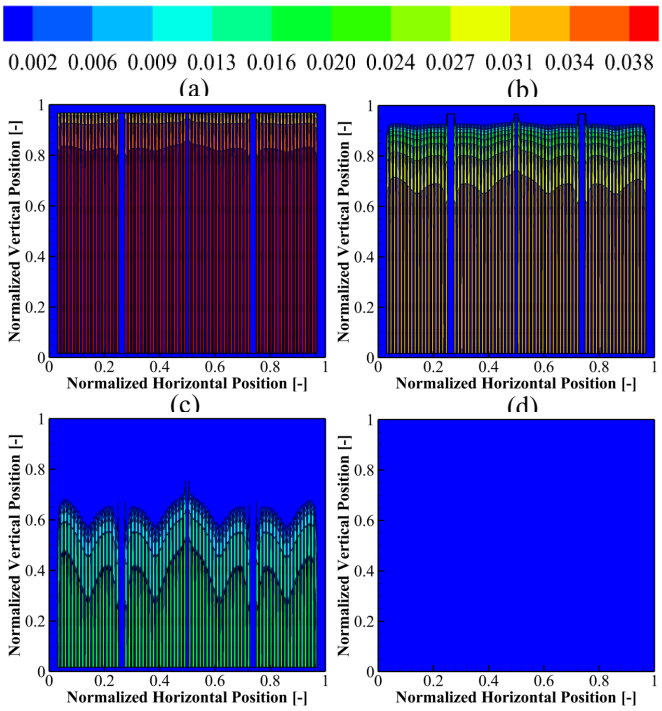

Fig. 15. Variation of liquid saturation in GDL/Channel interface at 0.3V: a) 80%, b) 60%, c) 40%, d) 20%.

In terms of water management, the transport of the liquid water within the cathode electrode and its removal from cathode channels are vital to keep up with the steady performance of the cell. Part of the water produced in the CLs is dissolved into the membrane while the rest of it passes through the GDL and being removed from the cathode channels. Figure 15 shows the contour of liquid saturation at the interface between the cathode GDL and the channels. More water is found at the interface for the high RH case (i.e., 80% RH) and a decreasing pattern can be observed in lowering the RH of cathode reactants (60% RH and 40% RH). One could observe that most of the liquid water pass through the GDL and subsequently be removed from the channels. The remaining liquid water would eventually cause flooding in the cathode electrode. When the RH is lowered to 20%, there is insignificant liquid retained at the interface between the CL and GDL. Therefore, as observed in Fig. 15, there is negligible liquid water at the interface between the GDLs and the channels.

5. Conclusion

The current study analysed the performance of a large PEMFC with multiple long straight channels. In this study, the cathode reactant at different RHs is fitted into the cathode channels aiming to investigate the effect of RHs on the overall cell performance. Numerical predictions ascertained that increasing humidification could pose a positive effect to the cell performance in both the ohmic and concentration polarization regions. Nonetheless, the enhancement in cell performance depends on the cell operational supply voltages (i.e., < 0.7V) and threshold of the RH value (i.e., 60%). Beyond the threshold RH value, further increasing the RH could only bring a marginal improvement to the cell performance. In comparing with the previous study of small PEMFCs at RMIT Laboratory, it is found that in parallel straight channels, the extended multiple long channels in the large cell help in removing the liquid water from the cell. With a better water removal mechanism, the delivery of reactants is also improved thus resulting in an enhanced cell performance. Similar improvement in the ohmic loss region is also found for the large cell. On the other hand, comparing with the small cell, the large cell suffers from a slight underperform in the activation loss region. Nonetheless, there is a significant improvement in the concentration loss region.

Acknowledgments

The authors would like to express sincere thanks to the members of the Reversible Fuel Cell team in the RMIT University.

References

[1] J.H. Hirschenhofer, D.B. Stauffer, and R.R. Engleman, Fuel Cells: A Handbook (US Department of Energy Office of Fossil Energy), 1994.

[2] C. Nevoloso, N. Campagna, M. Caruso, V. Castiglia, A.O.D. Tommaso and R. Miceli, “Interior permanent

magnet synchronous machine drive powered by fuel cell for automotive applications", 2020 9th International Conference on Renewable Energy Research and Applications (ICRERA), Glasgow, UK., IEEE, 2020, pp. 499-504, 27-30 September 2020.

[3] J. Larminie, and A. Dicks, Fuel Cell Systems Explained, John Wiley & Sons Ltd., 2003.

[4] B. Zafar, "Design of a renewable hybrid photovoltaic-electrolyze-PEM/fuel cell system using hydrogen gas", International Journal of Smart Grid, vol. 3, pp. 201-207, December 2019.

[5] N.E. Zakzouk, A. EI Dyasty, A. Ahmed and S.M. EI Safety, "Power flow control of a standalone photovoltaic-fuel cell-battery hybrid system", 2018 7th International Conference on Renewable Energy Research and Applications (ICRERA), Paris, France IEEE, 2018, pp. 431-436, 14-17 October 2018.

[6] H. Huang, N. Bristow, T.W. David, J. Kettle and G. Todeschini, "A novel computational model for organic PV cells and modules", International Journal of Smart Grid, vol. 4, pp. 157-163, December 2020.

[7] D. Guilbert, B. Yodwong, W. Kaewmanee and M. Phattanasak, "Power converters for hybrid renewable energy systems with hydrogen buffer storage: a short review", 2018 International Conference on Smart Grid, Nagasaki, Japan, IEEE, 2018, pp. 28-33, 4-6 December 2018.

[8] S. Gherairi, "Zero-emission hybrid electric system: estimated speed to prioritize energy demand for transport applications", International Journal of Smart Grid, vol. 3 No. 4, pp. 180-187. December 2019.

[9] M. Marefati, A. Shamel, R. Alayi, B. Gholaminia and H. Rohi, "Designing a PID controller to control a fuel cell voltage using the imperialist competitive algorithm", Advances in Science and Technology. Research Journal, vol. 10 (30), pp. 176-181, June 2016.

[10] M. Hossain, S.Z. Islam, A. Colley-Davies, and E. Adom, "Water dynamics inside a cathode channel of a polymer electrolyte membrane fuel cell", Renewable Energy, vol. 50, pp. 763-779, February 2013.

[11] K.N. Kim, D.H. Jeon, J.H. Nam, B.M. Kim, "Numerical study of straight-parallel PEM fuel cells at automotive operation", International Journal of Hydrogen Energy, vol. 37, pp. 9212-9227, April 2012.

[12] J.E. Dawes, N.S. Hanspal, O.A. Family, and A. Turan, "Three-dimensional CFD modelling of PEM fuel cells: an investigation into the effects of water flooding", Chemical Engineering Science, vol 64, pp. 2781-2794, June 2009.

[13] G. Zhang, Z. Bao, B. Xie, Y. Wang and K. Jiao, "Three-dimensional multi-phase simulation of PEM fuel cell considering the full morphology of metal foam flow field", International Journal of Hydrogen Energy, vol. 46, pp. 2978-2989, August 2020.

[14] K.W. Lum, and J.J. McGuirk, "Three-dimensional model of a complete polymer electrolyte membrane fuel cell – model formulation, validation, and parametric studies", Journal of Power Sources, vol. 143, pp. 103–124, April 2005.

[15] K. Jiao, B. Zhou, and P. Quan, "Liquid water transport in straight micro-parallel-channels with manifolds for PEM fuel cell cathode", Journal of Power Sources, vol. 157, pp. 226–243, March 2006.

[16] D.S. Falcao, P.J. Gomes, V.B. Oliveira, C. Pinho, and A.M.F.R. Pinto, "1D and 3D numerical simulations in PEM fuel cells", International Journal of Hydrogen Energy, vol. 36, pp. 12486 – 12498, September 2011.

[17] D.H. Jeon, S. Greenway, S. Shimpalee, and J.W. Van Zee, "The effect of serpentine flow-field designs on PEM fuel cell performance", International Journal of Hydrogen Energy, vol. 33, pp. 1052-1066, February 2008.

[18] E.E. Kahveci, and I. Taymaz, "Assessment of single-serpentine PEM fuel cell model developed by computational fluid dynamics", Fuel, vol. 217, pp. 51–58, April 2018.

[19] S. Li, and B. Sunden, "Effects of gas diffusion layer deformation on the transport phenomena and performance of PEM fuel cells with interdigitated flow fields", International Journal of Hydrogen Energy, vol. 43, pp. 16279–16292, August 2018.

[20] W.M. Yan, C.Y. Chen, S.C. Mei, C.Y. Soong, and F. Chen, "Effects of operating conditions on cell performance of PEM fuel cells with conventional or interdigitated flow field", Journal of Power Sources, vol. 162, pp. 1157–1164, August 2006.

[21] L. Wang, and H. Liu, "Performance studies of PEM fuel cells with interdigitated flow fields", Journal of Power Sources, vol. 134, pp.185–196, August 2004.

[22] Y. Wang, and C.Y. Wang, "A nonisothermal, two-phase model for polymer electrolyte fuel cells", Journal of the Electrochemical Society, vol. 153, pp. A1193-A1200, April 2006.

[23] S. Shimpalee, U. Beuscher, and J.W. Van Zee, "Analysis of GDL flooding effects on PEMFC performance", Electrochimica Acta, vol. 52, pp. 6748-6754, August 2007.

[24] L. Cindrella, A.M. Kannan, J.F. Lin, K. Saminathan, Y. Ho, C.W. Lin, and J. Wertz, "Gas diffusion layer for proton exchange membrane fuel cells – a review", Journal of Power Sources, vol. 194, pp. 146-160. April 2009.

[25] A. Iranzo, M. Munoz, E. Lopez, J. Pino, and F. Rosa, "Experimental fuel cell performance analysis under

different operating conditions and bipolar plate designs", International Journal of Hydrogen Energy, vol. 35, pp. 11437-11447, October 2010.

[26] N. Goswami, A.N. Mistry, J.B. Grunewald, T.F. Fuller and P.P. Mukherjee, "Corrosion-induced microstructural variability affects transport-kinetics interaction in PEM fuel cell catalyst layers", Journal of The Electrochemical Society, vol. 167, pp. 084519, May 2020.

[27] X.D. Wang, Y.Y. Duan, W.M. Yan, and F.B. Weng, "Effect of humidity of reactants on the cell performance of PEM fuel cells with parallel and interdigitated flow field design", Journal of Power Sources, vol. 176, pp. 247–258, January 2008.

[28] G. Zhang, X. Xie, B. Xie, Q. Du, and K. Jiao, "Large-scale multi-phase simulation of proton exchange membrane fuel cell", International Journal of Heat and Mass Transfer, vol. 130, pp. 555–563, March 2019.

[29] L. Xing, Q. Cai, C. Xu, C. Liu, K. Scott, and Y. Yan, "Numerical study of the effect of relative humidity and stoichiometric flow ratio on OEM (proton exchange membrane) fuel cell performance with various channel lengths: An anode partial flooding modelling", Energy, vol. 106, pp. 631-645, April 2016.

[30] R. Govindarasu, R. Parthiban and P.K. Bhaba, "Investigation of flow mal-distribution in proton exchange membrane fuel cell stack", International Journal of Renewable Energy Research, vol. 2, pp. 652-656, 2012.

[31] M. Arif, S.C.P. Cheung, and J. Andrews, "A systematic approach for matching simulated and experimental polarization curves for a PEM fuel cell", International Journal of Hydrogen Energy, vol. 45, pp. 2206-2223, January 2020.

[32] H. Askaripour, "Effect of operating conditions on the performance of a PEM fuel cell", International Journal of Heat and Mass Transfer, vol. 144, pp. 118705, September 2019.

[33] F.B. Weng, C.Y. Hsu, and C.W. Li, "Experimental investigation of PEM fuel cell aging under current cycling using segmented fuel cell", International Journal of Hydrogen Energy, vol. 35, pp. 3664-3675, April 2010.

[34] P.Y. Zhang, and Z.L. Liu, "Experimental study of the microbial fuel cell internal resistance", Journal of Power Sources, vol. 195, pp. 8013-8018, December 2010.

[35] A. Doddathimmaiah, and J. Andrews, "Theory, modelling and performance measurement of unitised regenerative fuel cells", International Journal of Hydrogen Energy, vol. 34, pp. 8157-8170, October 2009.

[36] ANSYS. ANSYS Fluent Fuel Cell Module manual, 2017.

[37] X. Huang, Z. Zhang, and J. Jiang, "Fuel cell technology for distributed generation: an overview", Journal of Fuel Cell Technology for Distributed Generation: An Overview", 2006 IEEE International Symposium on Industrial Electronics, Montreal, Quebec, Canada, vol. 2, IEEE, 2006, pp.1613-1618, 9-13 July 2006.

[38] S. Shimpalee, V. Lilavivat, H. Xu, J.R. Rowlett, C. Mittelsteadt, and J.W. Van Zee, "The effect of membrane properties on performance and transport inside polymer electrolyte membrane fuel cells", Journal of the Electrochemical Society, vol. 165, F1019-F1026, September 2018.

[39] R. Omrani and B. Shabani, "Can PTFE coating of gas diffusion layer improve the performance of URFCs in fuel cell-mode?", Energy Procedia, vol. 160, pp. 574-581, December 2018.

[40] J.H. Chun, K.T. Park, D.H. Jo, S.G. Kim, and S.H. Kim, "Numerical modelling and experimental study of the influence of GDL properties on performance in a PEMFC", International Journal of Hydrogen Energy, vol. 36, pp. 1837-1845, January 2010.

[41] S.A. Saco, R.T.K. Raj, and P. Karthikeyan, "A study on scaled up proton exchange membrane fuel cell with various flow channels for optimizing power output by effective water management using numerical technique", Energy, vol. 113, pp. 558–573, October 2016.

[42] T.E. Springer, T.A. Zowodzinski and S. Gottesfeld, "Polymer electrolyte fuel cell model", Journal of the Electrochemical Society, vol. 138, pp. 2334-2342, August 1991.